Common Origin of Green Luminescence in Carbon Nanodots and Graphene Quantum Dots
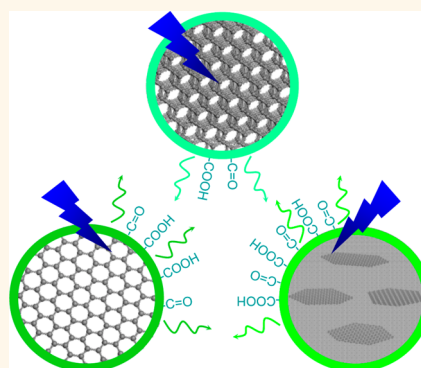
Lei Wang,[†] Shou-Jun Zhu,[‡] Hai-Yu Wang,[†,*] Song-Nan Qu,[⊥] Yong-Lai Zhang,[†] Jun-Hu Zhang,[‡] Qi-Dai Chen,[†] Huai-Liang Xu,[†] Wei Han,[§] Bai Yang,[‡,*] and Hong-Bo Sun[†,§,*]

[†]State Key Laboratory on Integrated Optoelectronics, College of Electronic Science and Engineering, [‡]State Key Laboratory of Supramolecular Structure and Materials, College of Chemistry, and [§]College of Physics, Jilin University, 2699 Qianjin Street, Changchun 130012, China and [⊥]State Key Laboratory of Luminescence and Applications, Changchun Institute of Optics, Fine Mechanics and Physics, Chinese Academy of Sciences, Changchun 130033, China. L.W. and S.Z. contributed equally to this work.

ABSTRACT Carbon nanodots (C-dots) synthesized by electrochemical ablation and small molecule carbonization, as well as graphene quantum dots (GQDs) fabricated by solvothermally cutting graphene oxide, are three kinds of typical green fluorescence carbon nanomaterials. Insight into the photoluminescence origin in these fluorescent carbon nanomaterials is one of the important matters of current debates. Here, a common origin of green luminescence in these C-dots and GQDs is unraveled by ultrafast spectroscopy. According to the change of surface functional groups during surface chemical reduction experiments, which are also accompanied by obvious emission-type transform, these common green luminescence emission centers that emerge in these C-dots and GQDs synthesized by bottom-up and top-down methods are unambiguously assigned to special edge states consisting of several carbon atoms on the edge of carbon backbone and functional groups with C=O (carbonyl and carboxyl groups). Our findings further suggest that the competition among various emission centers (bright edge states) and traps dominates the optical properties of these fluorescent carbon nanomaterials.

Fluorescent carbon nanomaterials, especially for carbon nanodots (C-dots) and graphene quantum dots (GQDs), have attracted much attention due to the superiority in resistance to photobleaching, low toxicity, excellent biocompatibility, low cost, and abundance of raw material in nature.[1−4] As a definition of ultrasmall fragments of carbon materials with tunable degree of carbonization, consisting of numerous functional groups on their surface, luminescent C-dots nowadays can be readily produced on a large scale by many approaches. As a result, these novel C-dot emitters have been used in a lot of optoelectronic application fields such as bioimaging, photocatalysis, photovoltaics, sensing, light-emitting diodes, and lasers.[5−18] Interestingly, most of the resulting C-dots exhibit blue or green emission, despite distinct techniques for fabrication, and these phenomena are also common for GQDs.

It is not surprising that various spectroscopic technologies have been considered and utilized as the most efficient means to propose a reasonable photoluminescence (PL) mechanism in fluorescent carbon nanomaterials.[19−27] Among these methods, ultrafast spectroscopy is a powerful tool for exploring the hidden information on electronic structure of materials.[28−30] According to ultrafast time-resolved fluorescence and carrier dynamics, Wen *et al.* suggested that there were intrinsic and extrinsic bands in C-dots.[29] Meanwhile, we found that independent bright molecule-like states were responsible for the fluorescence in GQDs *via* a series of ultrafast spectroscopy techniques, including femtosecond transient absorption spectroscopy.[30] Moreover, we have recently directly observed quantum-confined graphene-like electronic states in graphene oxide and photothermally reduced graphene oxide *via* transient absorption

spectroscopy and suggested that the transient excited-state absorption signals could be corresponding to some special oxygen-containing functional groups.[31] Inspired by this work, we wonder whether there exists any common relationship between green PL and special functional groups in both C-dots and GQDs, and what kind of role the carbon backbone plays in these fluorescent carbon nanomaterials.

The chief problem we need to face is a variety of C-dots and GQDs, which makes it hard to correctly evaluate the whole picture about their PL mechanism. To simplify this complex question as much as possible, the carbon nanomaterials with small size distribution and high PL quantum yield (QY) are crucial and necessary. This is due to the fact that higher sample quality and simpler physical process can be expected. As a result, ease of production, high quality, and output of C-dots and GQDs will give us a better opportunity to study their unique optical properties as a significant breakthrough for understanding the photophysics of fluorescent carbon nanomaterials.

Hence, C-dots and GQDs adopted here are typical and superior in quality.[5,13,32] C-dots synthesized by electrochemical ablation of graphite rod electrodes (top-down method) have high graphitic crystallinity,[6,13] and C-dots synthesized by microwave-assisted small molecule carbonization (bottom-up method) usually possess high PL QY.[5] GQDs fabricated by a two-step method combining "top-down" cutting graphene oxide and separation routes abandon a redundant carbon matrix, in return to which high PL emission appears.[30,32] In combination of femtosecond time-resolved spectroscopy and FT-IR spectroscopy before and after surface chemical reduction treatment, we explore the common PL origin of these C-dots and GQDs in detail and further identify the functional groups bearing responsibility for fluorescence emission. Our findings highlight the common transient species in typical green fluorescence C-dots and GQDs, regardless of fabrication methods.

RESULTS AND DISCUSSION

Figure 1 shows the steady-state absorption and emission spectra of these typical green fluorescence carbon nanomaterials. Interestingly, the three samples possess very different absorption in the ultraviolet to visible range, but their normalized PL peaks are all located at the green region at 400 nm excitation. According to the high-resolution TEM images for the three samples, as shown in Supporting Information Figure S1, electrochemically synthesized C-dots have the highest graphitic crystallinity and largest size distribution in the range of 1−9 nm, with an average value of ∼5 nm. This could lead to a broad and structureless absorption in the visible range. Smaller size distribution in microwave-synthesized C-dots (1−5 nm) and disk-like GQDs fabricated by solvothermal synthesis
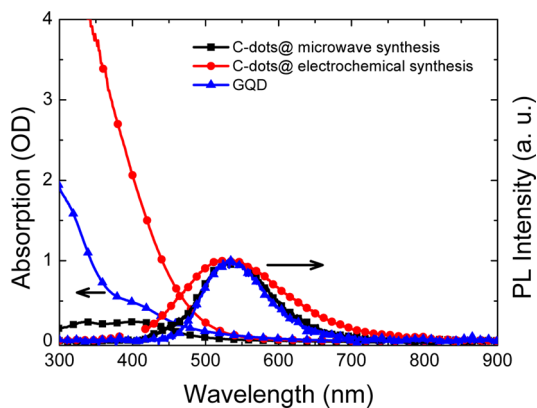

Figure 1. Steady-state absorption and emission spectra of green fluorescence C-dots and GQDs at 400 nm excitation.

(3−5 nm) leads to narrower full width at half-maximum (fwhm) in the normalized PL spectra, and at the same time, some subtle band structures also appear in steady-state absorption spectra. For solvothermally synthesized GQDs, we have assigned these subtle bands to independent molecule-like states.[30] Similar states appearing in microwave-synthesized C-dots could reflect a common origin. The resulting PL QY (see details in Supporting Information) in microwave-synthesized C-dots (11.43%) and solvothermally synthesized GQDs (9.81%) is enhanced to a great extent, in comparison with electrochemically synthesized C-dots (0.81%).

In order to shed light on these mysteries, femtosecond transient absorption spectroscopy was used at first for these three samples at 400 nm excitation (Figure 2). Usually, there are three kinds of spectral features in the TA spectrum. After the pump light excitation, due to the Pauli exclusion principle, the filling of quantized electronic states will lead to the bleaching of the corresponding optical transitions from ground state to excited state, which is named ground-state bleaching (GSB). On the other hand, the photoexcited electrons in the excited states could further absorb probe light to higher levels or return to ground state by stimulated radiation due to the disturbance of probe light, which is the so-called excited-state absorption (ESA) and stimulated emission (SE), respectively. Among the features, only excited-state absorption has positive signals, the other has negative signals. All of these features reflect the information about the change of photogenerated carrier populations in corresponding energy levels.

For the typical TA spectra of microwave-synthesized C-dots, there is a small negative signal at around 420 nm, which corresponds to the energy band structure in the steady-state absorption spectrum at similar wavelength. Therefore, we assign this state to the ground-state bleaching signal. At longer wavelength, there is a larger negative signal, which is in the range of their green PL. Thus, this state is assigned to stimulated
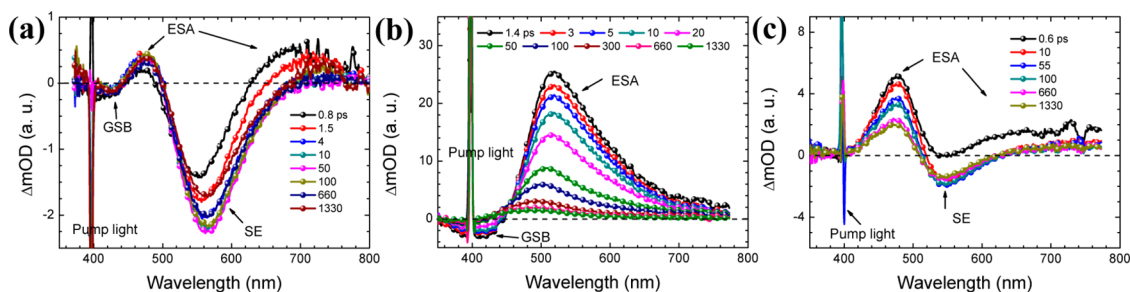
Figure 2. TA spectra for (a) microwave-synthesized C-dots, (b) electrochemically synthesized C-dots, and (c) solvothermally synthesized GQDs at 400 nm excitation. GSB, ground-state bleaching; ESA, excited-state absorption; SE, stimulated emission.

emission (SE). Despite the spectral superposition in each TA spectra, it is still amazing that these transient features in the three kinds of carbon nanomaterials can be attributed to the same model. The main difference is the strength of stimulated emission. It seems that stronger PL QY leads to larger stimulated emission signal.

For short time scale (first several picoseconds), a transient double difference spectrum is used to obtain the information hidden by overlapping of different spectral signals. These double difference spectra of C-dots and GQDs give clearer ground-state bleaching signals at around 400 nm and similar excited-state absorption, if ignoring the cupped shape at 490 nm (Figure 3a). It indicates that the fast disappearance of this positive absorption band is accompanied by re-covering of the same ground-state bleaching (see latter comparative analysis between TA and time-resolved PL experiments). Furthermore, a deeper cupped shape appears in microwave-synthesized C-dots, besides the exactly same absorption band in the red side of the probe window. It even already becomes a negative signal, compared with that in solvothermally synthesized GQDs. Hence, we can safely assign this cupped signal to a fast stimulated emission component, corresponding to the ground state at around 400 nm. On the other hand, for a long nanosecond time scale in TA, the blue and red sides of excited-state absorption for electrochemically synthesized C-dots are consistent with that of GQDs, also except for the PL region (Figure 3b). For microwave-synthesized C-dots, remarkably long lifetime stimulated emission signal is accompanied by a ground-state bleaching signal at around 420 nm. This long lifetime ground state is in agreement with the green fluorescence emission center found in GQDs. As stated above, there is a serious spectral overlapping in TA spectra, that is, ground-state bleaching, excited-state absorption, and stimulated emission. However, they can be separated according to the steady-state spectra. Briefly, by subtracting the steady-state PL spectrum from the TA spectrum, the combination of excited-state absorption and ground-state bleaching can be obtained. Then, we assumed that the excited-state absorption has a Gaussian shape and used a Gaussian line shape to fit the obtained spectrum. The best fitting
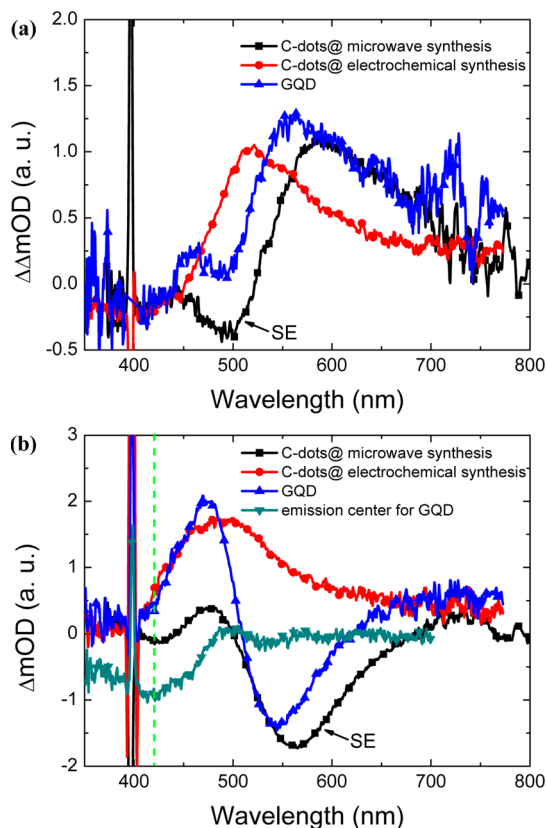

Figure 3. (a) Double difference spectra for microwave-synthesized C-dots (between 0.8 and 10 ps), electrochemically synthesized C-dots (between 1.4 and 5 ps), and solvothermally synthesized GQDs (between 0.6 and 5 ps). **(b)** TA spectra at nanosecond time scale (1.33 ns) for these C-dots and GQDs. For details on the emission center for GQDs, see our previous work.[30] The vertical dashed line is located at 420 nm.

Gaussian line shape represents the pure excited-state absorption. Finally, after subtracting this pure excited-state absorption component from the spectrum including both excited-state absorption and ground-state bleaching information, we obtained a pure ground-state bleaching signal corresponding to the green fluorescence. The detailed deduction for GQDs is seen in our previous work.[30] These results unambiguously indicate that these green fluorescence C-dots and GQDs, no matter if synthesized by small molecule carbonization, electrochemical ablation, or solvothermal

synthesis, have the same excited-state behaviors. The only difference is the proportion of radiative recombination in the whole relaxation processes of photogenerated carriers.

As a necessary complement, femtosecond time-resolved PL experiments are performed at 400 nm excitation to observe the pure radiative recombination processes (Figure 4). All the fluorescence transients are probed at PL peaks and are well fitted with multi-exponential functions; the best-fit parameters are listed in Table 1. For the microwave-synthesized C-dots and GQDs, both of them have common short lifetime components of 1−2 ps and long lifetime components of 4−5 ns, except that there is an additional decay component of ~110 ps in GQDs. This indicates that, in comparison with microwave-synthesized C-dots, solvothermally synthesized GQDs have some deeper trap levels, which decrease PL QY. It is worth noting that these average PL lifetimes, including all the lifetime components, only provide the information of relative emission strength, which can not correlate with PL QY precisely. In addition, for both microwave-synthesized C-dots and solvothermally synthesized GQDs, wavelength-dependent PL dynamics ranging from the blue side to the red side of PL also possess similar decay trend (Figure S2). There is no fast decay in the red side of the green fluorescence (wavelength beyond 520 nm), but in the blue side, shorter wavelength has a larger fast decay component. We previously assigned the fast/long lifetime to an intrinsic state/molecule-like state in GQDs.[30] These time-resolved PL dynamics demonstrate that the same conclusions are also

Figure 4. Femtosecond time-resolved PL dynamics of C-dots (probed at 520 nm) and GQDs (probed at 530 nm) at 400 nm excitation.

TABLE 1. Multiexponential Fitting for Femtosecond Time-Resolved Fluorescence Dynamics

samples	τ_1 (ps)	τ_2 (ps)	τ_3 (ps)	τ_{ave} (ps)
microwave-synthesized C-dots	1.4 (25%)		4700 (75%)	3525
electrochemically synthesized C-dots	1.0 (47%)	16.6 (30%)	430 (23%)	104
solvothermally synthesized GQDs	1.9 (23%)	110 (17%)	4000 (60%)	2419

suitable for microwave-synthesized C-dots, in which their PL of the intrinsic state and molecule-like state is even stronger. For electrochemically synthesized C-dots, all three lifetime components are shorter, which leads to an average PL lifetime of only ~100 ps, 1 order of magnitude faster than the other two samples. This indicates that nonradiative recombination processes are dominated in electrochemically synthesized C-dots, which leads to the lowest PL QY.

As long as these characterization dynamics in time-resolved PL or TA represent the same excited-state energy level, the comparison with each other is powerful evidence for identifying the relaxation channel of excited-state electrons in the complex photophysical process. For a short time scale, the kinetics of three different characterization wavelengths, which are the blue side of green fluorescence (470 or 480 nm in PL), ground-state bleaching (410 nm in TA), and excited-state absorption (650 or 680 nm in TA), are very consistent with that shown in Figure S3. In order to avoid the influence of fluorescence signal, the wavelength of 650 or 680 nm in TA is adopted to represent the red side of the excited-state absorption signal. This accounts for the origin of the blue side of the green fluorescence around 470 nm. Namely, this part of PL arises from a ground state (intrinsic state), located around 400 nm, with the corresponding red side of excited-state absorption. Due to the fast decay, the photoluminescence quantum yield of this state is estimated to be very low, and it has almost no contribution to the steady-state fluorescence at 400 nm excitation. For the long time scale, the dynamics of the long lifetime of the blue side of the excited-state absorption signal (470 or 520 nm in TA) are indeed the same as that of red side of PL (600 nm in PL) shown in Figure S4. This indicates that the strong green fluorescence originates from another state, which corresponds to the blue side of the excited-state absorption. This state also has a ground state which is located at around 420 nm (Figure 3b).

Considering the degree of carbonization and plenty of functional groups on the surface of C-dots and GQDs, the common photophysics on the basis of our transient studies are unraveled: photogenerated carriers are at first stored in the carbon backbone, then leak fast into any possible emission states (special structure consisting of carbon atoms and functional groups) and traps (meaningless structures), in which graphitic crystallinity plays the role of temporary reservoir. In this mechanism, increased degree of graphitic crystallinity or carbonization will lead to better photostability, as well as more drastic competition among different relaxation channels created by irregular carbonization or surface states which are out of control. To the best of our knowledge, these surface states with functional groups in most carbon nanomaterials are still disordered and mainly
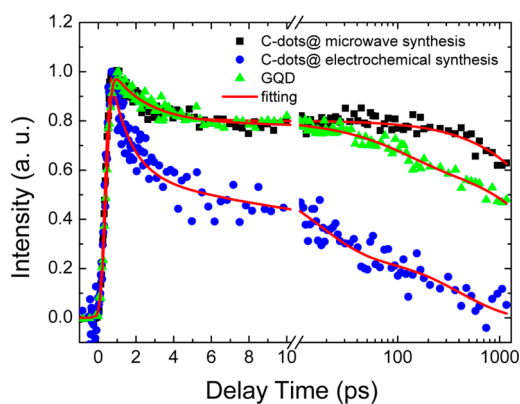
dependent on synthesis processes and post-treatments until now.

The characteristic absorption bands of surface functional groups in these C-dots and GQDs can be detected by FT-IR (Figure 5). For example, there are stretching vibrations of O−H and N−H at 3100−3500 cm^{-1}, C−H at 2923 and 2850 cm^{-1}, bending vibrations of CH$_2$ at 1350−1460 cm^{-1}, vibrational absorption band of C=O at 1635 cm^{-1}, and an epoxide band at 1048 cm^{-1}.[5,7,33] To gain an insight into the special surface states probably responsible for green PL in these carbon nanomaterials, surface chemical reduction treatments in C-dots and GQDs are further carried out (Figure 5, red line). Taking reduced microwave-synthesized C-dots as an example, after reduction, the strength of absorption bands of C−OH and C=O is 1/2 and 1/3 remaining, respectively, while the absorption band of CH$_2$ is broadened and increases by 2.5 times. This phenomenon of loss of an absorption band of C−OH that is smaller than that of C=O can be explained by the transformation from carbonyl and epoxy to −OH groups in the reduction process.[33] Thus,

the decreasing of carboxyl groups becomes the main reason for the loss of an absorption band of C−OH. These FT-IR spectra before surface reduction also show that the hydroxyl group and carboxyl group are dominant in all samples. The main difference among these samples is the category and quantity of other surface functional groups, such as in the range of 800−1500 cm^{-1}, in which it includes numerous characterization absorption bands (i.e., C−O, C−H, even C−N).[7,33] All of these surface functional groups may become different competition channels, including radiative and nonradiative processes. Hence, with more surface functional groups, except that contributing to green emission, lower green PL QY can be expected, as electrochemically synthesized C-dots presented here. In contrast, a more unitary emission center with larger quantity will certainly result in higher PL QY. This not only explains the cases of microwave-synthesized C-dots and solvothermally synthesized GQDs well but also can extend to the highly photoluminescent C-dots with blue emission.[7]

In the meantime, the resulting steady-state PL spectra at 400 nm excitation are changed during this reduction process (Figure S5). By subtracting the PL spectrum before reduction from that at different reduction
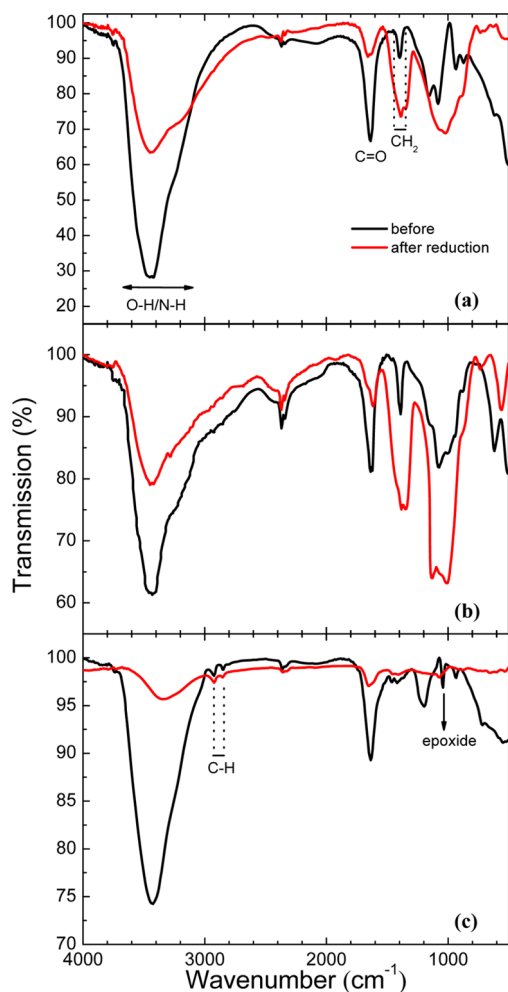

Figure 5. FT-IR spectra of (a) microwave-synthesized C-dots, (b) electrochemically synthesized C-dots, and (c) solvothermally synthesized GQDs.
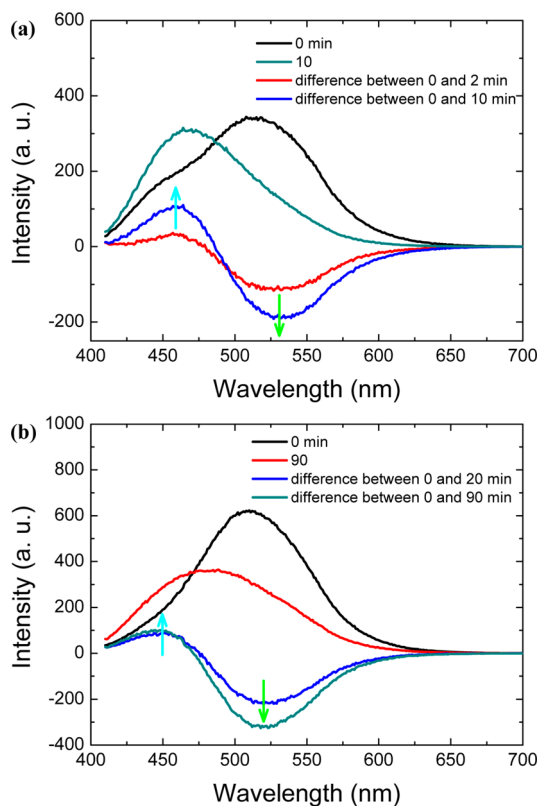

Figure 6. Steady-state PL difference spectra of (a) reduced microwave-synthesized C-dots and (b) reduced solvothermally synthesized GQDs at different reduced times. In this difference spectrum, negative signal represents disappeared PL signal, and positive signal represents emerged PL in the reduction processes. The arrows indicate the trend of PL change.

times, the information on the change of emission type is more obvious (Figure 6). We can see that green emission part centered at 530 nm gradually disappears (negative signal) and a new blue emission centered at 460 nm appears (positive signal). Both microwave-synthesized C-dots and solvothermally synthesized GQDs have similar emission-type transformation during the surface chemical treatments. For electrochemically synthesized C-dots, since some undesired depositions occur, as well as the low PL QY in the same excitation condition, its steady-state PL spectra during the reduction process are not recorded. Interestingly, we further find that all the C-dots and GQDs with green emission exhibit the same pH-dependent PL behavior (Figure S6). The intensities of green emission decrease in the solution of high or low pH value but almost remain constant in a solution of pH 4−10. This reflects another common PL property of their green emission. That is, the pH-dependent behaviors at specific ranges may contribute to the protonation/deprotonation of carboxyl groups, which affect the PL center of the green emissions. In a word, all of these steady-state experiments also confirm the common contribution of C=O functional groups, especially for carboxyl groups at the edge on the emission of fluorescent carbon nanomaterials.

Associating these changes in steady-state spectroscopy with their transient processes, it further means that when these local molecule-like states containing carboxyl groups and carbonyl groups are formed on the surface of carbon nanomaterials, it will certainly lead to common transient species in transient absorption spectroscopy. Furthermore, recent study on green photoluminescence GQDs *via* steady-state PL analysis

and high-resolution transmission microscopy strongly suggested that green PL originated from disordered edge states.[34] Since both carboxyl groups and carbonyl groups only emerge on the edge of the carbon backbone, our findings not only support this evidence but also depict the possible category of edge states in carbon nanomaterials. It is worth noting that sole C=O functional groups are useless for green emission, like in many small molecules and graphene-oxide-containing carboxyl groups at its edge.[35] However, relying on the carbon backbone in these carbon nanomaterials, the formation of some special conformations can be facilitated by combination of carboxyl groups and carbonyl groups in the vicinity at the edge of the carbon nanomaterials. In another word, the hybridization of the carbon backbone and these chemical groups forms the green PL centers. These special edge states are the common origins of green emission.

CONCLUSIONS

In summary, formation of special molecule-like states in carbon nanodots and graphene quantum dots are demonstrated to be responsible for their green fluorescence. Since these molecule-like states contain carboxyl groups and carbonyl groups, they are parts of so-called edge states. Special molecule conformations consisting of these functional groups and several edge carbon atoms of the carbon backbone can be expected. Besides, due to the variety of possible edge states, some edge states could be nonradiative states, namely, so-called traps. Hence, the competition among different emission centers and traps dominates the optical properties of carbon nanomaterials.

MATERIALS AND METHODS

Sample Preparation. For microwave-synthesized C-dots, citric acid and urea were used in a one-step microwave synthesis route.[5] For electrochemically synthesized C-dots, graphite rods were adopted as both anode and cathode, as well as the carbon source in a typical electrochemical synthesis.[13] For solvothermally synthesized GQDs, a one-step solvothermal route from graphene oxide is implemented.[32] For surface chemical reduction experiments, 50 mg of $NaBH_4$ was added into 3 mL of C-dots or GQDs, with the reaction mixture stirred at room temperature. Steady-state PL spectra of this reduced sample are recorded at desired times. After complete reaction, the product was subjected to dialysis to completely remove ions. The resulting product was used in FT-IR analysis.

Femtosecond Transient Absorption Setup. In the transient absorption setup, a mode-locked Ti:sapphire laser/amplifier system (Solstice, Spectra-Physics) was used. The output of the amplifier of 1.5 mJ pulse energy, 100 fs pulse width, 250 Hz repetition rate (this low frequency is set for matching the signal collection system), at 800 nm wavelength was split into two parts; the stronger beam was used to generate desired excitation light. In traditional 400 nm excitation experiments, 400 nm pump pulses directly doubled from 800 nm laser pulses. The broad-band white-light probe pulses were from 400 to 850 nm generated from 2 mm thick water. The transient absorption data were collected by a fiber-coupled spectrometer connected to a computer. The group velocity dispersion of the transient spectra

was compensated by a chirp program. In all ultrafast experiments, samples were stored in a 2 mm cuvette, in which microwave-synthesized C-dots and solvothermally synthesized GQDs were dissolved in water, and electrochemically synthesized C-dots were dissolved in ethanol. All measurements were preformed at room temperature. Pump-power-dependent measurements were carried out. In the acceptable range (0.1− 0.6 mJ/cm^2), no pump-intensity-dependent dynamics were observed in 400 nm excitation.

Time-Resolved Fluorescence Experiments. Subpicosecond time-resolved emission was measured by the femtosecond fluorescence upconversion method. A mode-locked Ti:sapphire laser/amplifier system (Solstice, Spectra-Physics) was used. The output of the amplifier of 1.5 mJ pulse energy, 100 fs pulse width, 1 kHz repetition rate, at 800 nm wavelength is split into two parts; the stronger beam was used to generate excitation light. The resulting fluorescence was collected and focused onto a 1 mm thick BBO crystal with a cutting angle of 35°. The other part of the regenerative amplifier output was sent into an optical delay line and served as the optical gate for the upconversion of the fluorescence. The generated sum frequency light was then collimated and focused into the entrance slit of a 300 mm monochromator. A UV-sensitive photomultiplier tube 1P28 (Hamamatsu) was used to detect the signal. The fwhm of instrument response function was about 400 fs.

REFERENCES AND NOTES

1. Baker, S. N.; Baker, G. A. Luminescent Carbon Nanodots: Emergent Nanolights. *Angew. Chem., Int. Ed.* **2010**, *49*, 6726–6744.

2. Li, H. T.; Kang, Z. H.; Liu, Y.; Lee, S. T. Carbon Nanodots: Synthesis, Properties and Applications. *J. Mater. Chem.* **2012**, *22*, 24230–24253.

3. Zhu, S. J.; Tang, S. J.; Zhang, J. H.; Yang, B. Control the Size and Surface Chemistry of Graphene for the Rising Fluorescent Materials. *Chem. Commun.* **2012**, *48*, 4527–4539.

4. Shen, J. H.; Zhu, Y. H.; Yang, X. L.; Li, C. Z. Graphene Quantum Dots: Emergent Nanolights for Bioimaging, Sensors, Catalysis and Photovoltaic Devices. *Chem. Commun.* **2012**, *48*, 3686–3699.

5. Qu, S. N.; Wang, X. Y.; Lu, Q. P.; Liu, X. Y.; Wang, L. J. A Biocompatible Fluorescent Ink Based on Water-Soluble Luminescent Carbon Nanodots. *Angew. Chem., Int. Ed.* **2012**, *51*, 12215–12218.

6. Li, H. T.; He, X. D.; Kang, Z. H.; Huang, H.; Liu, Y.; Liu, J. L.; Lian, S. Y.; Tsang, C. H. A.; Yang, X. B.; Lee, S. T. Water-Soluble Fluorescent Carbon Quantum Dots and Photocatalyst Design. *Angew. Chem., Int. Ed.* **2010**, *49*, 4430–4434.

7. Zhu, S. J.; Meng, Q. N.; Wang, L.; Zhang, J. H.; Song, Y. B.; Jin, H.; Zhang, K.; Sun, H. C.; Wang, H. Y.; Yang, B. Highly Photoluminescent Carbon Dots for Multicolor Patterning, Sensors, and Bioimaging. *Angew. Chem., Int. Ed.* **2013**, *52*, 3953–3957.

8. Wang, J.; Wang, C. F.; Chen, S. Amphiphilic Egg-Derived Carbon Dots: Rapid Plasma Fabrication, Pyrolysis Process, and Multicolor Printing Patterns. *Angew. Chem., Int. Ed.* **2012**, *51*, 9297–9301.

9. Zhu, C. Z.; Zhai, J. F.; Dong, S. J. Bifunctional Fluorescent Carbon Nanodots: Green Synthesis *via* Soy Milk and Application as Metal-Free Electrocatalysts for Oxygen Reduction. *Chem. Commun.* **2012**, *48*, 9367–9369.

10. Kong, B.; Zhu, A. W.; Ding, C. Q.; Zhao, X. M.; Li, B.; Tian, Y. Carbon Dot-Based Inorganic−Organic Nanosystem for Two-Photon Imaging and Biosensing of pH Variation in Living Cells and Tissues. *Adv. Mater.* **2012**, *24*, 5844–5848.

11. Ma, Z.; Zhang, Y. L.; Wang, L.; Ming, H.; Li, H. T.; Zhang, X.; Wang, F.; Liu, Y.; Kang, Z. H.; Lee, S. T. Bioinspired Photoelectric Conversion System Based on Carbon-Quantum-Dot-Doped Dye-Semiconductor Complex. *ACS Appl. Mater. Interfaces* **2013**, *5*, 5080–5084.

12. Mirtchev, P.; Henderson, E. J.; Soheilnia, N.; Yip, C. M.; Ozin, G. A. Solution Phase Synthesis of Carbon Quantum Dots as Sensitizers for Nanocrystalline TiO_2 Solar Cells. *J. Mater. Chem.* **2012**, *22*, 1265–1269.

13. Zhang, Y. L.; Wang, L.; Zhang, H. C.; Liu, Y.; Wang, H. Y.; Kang, Z. H.; Lee, S. T. Graphitic Carbon Quantum Dots as a Fluorescent Sensing Platform for Highly Efficient Detection of Fe^{3+} Ions. *RSC Adv.* **2013**, *3*, 3733–3738.

14. Wang, F.; Chen, Y. H.; Liu, C. Y.; Ma, D. G. White Light-Emitting Devices Based on Carbon Dots' Electroluminescence. *Chem. Commun.* **2011**, *47*, 3502–3504.

15. Guo, X.; Wang, C. F.; Yu, Z. Y.; Li, C.; Chen, S. Facile Access to Versatile Fluorescent Carbon Dots toward Light-Emitting Diodes. *Chem. Commun.* **2012**, *48*, 2692–2694.

16. Zhang, X. Y.; Zhang, Y.; Wang, Y.; Kalytchuk, S.; Kershaw, S. V.; Wang, Y. H.; Wang, P.; Zhang, T. Q.; Zhao, Y.; Zhang, H. Z.; *et al.* Color-Switchable Electroluminescence of Carbon Dot Light-Emitting Diodes. *ACS Nano* **2013**, *7*, 11234–11241.

17. Zhang, W. F.; Tang, L. B.; Yu, S. F.; Lau, S. P. Observation of White-Light Amplified Spontaneous Emission from Carbon Nanodots under Laser Excitation. *Opt. Mater. Express* **2012**, *2*, 490–495.

18. Zhang, W. F.; Zhu, H.; Yu, S. F.; Yang, H. Y. Observation of Lasing Emission from Carbon Nanodots in Organic Solvents. *Adv. Mater.* **2012**, *24*, 2263–2267.

19. Cao, L.; Meziani, M. J.; Sahu, S.; Sun, Y. P. Photoluminescence Properties of Graphene *versus* Other Carbon Nanomaterials. *Acc. Chem. Res.* **2013**, *46*, 171–180.

20. Gan, Z. X.; Xiong, S. J.; Wu, X. L.; Xu, T.; Zhu, X. B.; Gan, X.; Guo, J. H.; Shen, J. C.; Sun, L. T.; Chu, P. K. Mechanism of Photoluminescence from Chemically Derived Graphene Oxide: Role of Chemical Reduction. *Adv. Opt. Mater.* **2013**, *1*, 926–932.

21. Wang, X.; Cao, L.; Yang, S. T.; Lu, F. S.; Meziani, M. J.; Tian, L. L.; Wang, K. W.; Bloodgood, M. A.; Sun, Y. P. Bandgap-like Strong Fluorescence in Functionalized Carbon Nanoparticles. *Angew. Chem.* **2010**, *122*, 5438–5442.

22. Pan, D. Y.; Zhang, J.; Li, Z.; Wu, M. H. Hydrothermal Route for Cutting Graphene Sheets into Blue-Luminescent Graphene Quantum Dots. *Adv. Mater.* **2010**, *22*, 734–738.

23. Liu, F.; Jang, M. H.; Ha, H. D.; Kim, J. H.; Cho, Y. H. Facile Synthetic Method for Pristine Graphene Quantum Dots and Graphene Oxide Quantum Dots: Origin of Blue and Green Luminescence. *Adv. Mater.* **2013**, *25*, 3657–3662.

24. Wang, X.; Cao, L.; Lu, F. S.; Meziani, M. J.; Li, H. T.; Qi, G.; Zhou, B.; Harruff, B. A.; Kermarrec, F.; Sun, Y. P. Photoinduced Electron Transfers with Carbon Dots. *Chem. Commun.* **2009**, 3774–3776.

25. Lin, F.; Pei, D. J.; He, W. N.; Huang, Z. X.; Huang, Y. J.; Guo, X. Q. Electron Transfer Quenching by Nitroxide Radicals of the Fluorescence of Carbon Dots. *J. Mater. Chem.* **2012**, *22*, 11801–11807.

26. Bao, L.; Zhang, Z. L.; Tian, Z. Q.; Zhang, L.; Liu, C.; Lin, Y.; Qi, B. P.; Pang, D. W. Electrochemical Tuning of Luminescent Carbon Nanodots: From Preparation to Luminescence Mechanism. *Adv. Mater.* **2011**, *23*, 5801–5806.

27. Yu, P.; Wen, X. M.; Toh, Y. R.; Tang, J. Temperature-Dependent Fluorescence in Carbon Dots. *J. Phys. Chem. C* **2012**, *116*, 25552–25557.

28. Exarhos, A. L.; Turk, M. E.; Kikkawa, J. M. Ultrafast Spectral Migration of Photoluminescence in Graphene Oxide. *Nano Lett.* **2013**, *13*, 344–349.

29. Wen, X. M.; Yu, P.; Toh, Y. R.; Hao, X. T.; Tang, J. Intrinsic and Extrinsic Fluorescence in Carbon Nanodots: Ultrafast Time-Resolved Fluorescence and Carrier Dynamics. *Adv. Opt. Mater.* **2013**, *1*, 173–178.

30. Wang, L.; Zhu, S. J.; Wang, H. Y.; Wang, Y. F.; Hao, Y. W.; Zhang, J. H.; Chen, Q. D.; Zhang, Y. L.; Han, W.; Yang, B.; *et al.* Unraveling Bright Molecule-like State and Dark Intrinsic State in Green-Fluorescence Graphene Quantum Dots *via* Ultrafast Spectroscopy. *Adv. Opt. Mater.* **2013**, *1*, 264–271.

31. Wang, L.; Wang, H. Y.; Wang, Y.; Zhu, S. J.; Zhang, Y. L.; Zhang, J. H.; Chen, Q. D.; Han, W.; Xu, H. L.; Yang, B.; *et al.* Direct Observation of Quantum-Confined Graphene-like States and Novel Hybrid States in Graphene Oxide by Transient Spectroscopy. *Adv. Mater.* **2013**, *25*, 6539–6545.

32. Zhu, S. J.; Zhang, J. H.; Liu, X.; Li, B.; Wang, X. F.; Tang, S. J.; Meng, Q. N.; Li, Y. F.; Shi, C.; Hu, R.; *et al.* Graphene Quantum Dots with Controllable Surface Oxidation, Tunable Fluorescence and Up-Conversion Emission. *RSC Adv.* **2012**, *2*, 2717–2720.

33. Zhu, S. J.; Zhang, J. H.; Tang, S. J.; Qiao, C. Y.; Wang, L.; Wang, H. Y.; Liu, X.; Li, B.; Li, Y. F.; Yu, W. L.; *et al.* Surface Chemistry Routes to Modulate the Photoluminescence of Graphene Quantum Dots: From Fluorescence Mechanism to Up-Conversion Bioimaging Applications. *Adv. Funct. Mater.* **2012**, *22*, 4732–4740.

34. Lingam, K.; Podila, R.; Qian, H. J.; Serkiz, S.; Rao, A. M. Evidence for Edge-State Photoluminescence in Graphene Quantum Dots. *Adv. Funct. Mater.* **2013**, *23*, 5062–5065.

35. Galande, C.; Mohite, A. D.; Naumov, A. V.; Gao, W.; Ci, L. J.; Ajayan, A.; Gao, H.; Srivastava, A.; Weisman, R. B.; Ajayan, P. M. Quasi-Molecular Fluorescence from Graphene Oxide. *Sci. Rep.* **2011**, *1*, 85.